

## Original Article

**Cite this article:** Chatterjee A, Chalapathi Rao NV, Pandey R, and Pandey A (2023) Mantle transition zone-derived eclogite xenolith entrained in a diamondiferous Mesoproterozoic (~1.1 Ga) kimberlite from the Eastern Dharwar Craton, India: evidence from a coesite, K-omphacite, and majoritic garnet assemblage. *Geological Magazine* **160**: 874–887. <https://doi.org/10.1017/S0016756822001315>

Received: 5 July 2022

Revised: 8 December 2022

Accepted: 23 December 2022

First published online: 15 February 2023



**Keywords:**

mantle transition zone; ultra-deep subduction; kimberlite; Dharwar craton

**Author for correspondence:**

N. V. Chalapathi Rao, Email: [nvcrao@bhu.ac.in](mailto:nvcrao@bhu.ac.in)

# Mantle transition zone-derived eclogite xenolith entrained in a diamondiferous Mesoproterozoic (~1.1 Ga) kimberlite from the Eastern Dharwar Craton, India: evidence from a coesite, K-omphacite, and majoritic garnet assemblage

Amitava Chatterjee<sup>1,2</sup> , N. V. Chalapathi Rao<sup>2</sup> , Rohit Pandey<sup>2</sup> and Ashutosh Pandey<sup>1</sup>

<sup>1</sup>Department of Earth Sciences, School of Physical, Chemical and Applied Sciences, Pondicherry University, Puducherry 605014, India and <sup>2</sup>Department of Geology, Institute of Science, Banaras Hindu University, Varanasi 221005, India

**Abstract**

Subduction-related kimberlite-borne eclogite xenoliths of the Precambrian age may provide significant information about the evolution and recycling of a subducting crust as exhumed/orogenic eclogites of the pre-Mesoproterozoic time-frame are globally rare. In this paper, we report a kimberlite-borne eclogite xenolith from the diamondiferous Kalyandurg kimberlite cluster of the Eastern Dharwar Craton, India, which contains a plethora of ultra-high-pressure minerals such as coesite, majoritic garnet, and supersilicic K-rich omphacite. The presence of these ultra-high-pressure minerals is confirmed by *in situ* X-ray diffractometry, laser Raman spectra and electron probe microanalysis. The presence of coesite undisputedly pinpoints a subduction origin for the eclogite at ~2.8 GPa pressure, which corresponds to ~100 km depth. The geothermobarometric estimations involving garnet–omphacite–kyanite–coesite reveal that such an eclogitic assemblage equilibrated at ~5–8 GPa (~175–280 km) pressure during ultra-deep subduction. The textural relationship between omphacite, coarse-grained garnet and majoritic garnet coupled with the laser Raman spectra and geobarometric estimations obtained from the majoritic garnet demonstrate that the majoritic garnet formed at ~8–19 GPa (~280–660 km) owing to disassociation of omphacite and coarse-grained garnet to majoritic garnet during increment of pressure up to the mantle transition zone. Thus, the mineralogical and geothermobarometric data suggest that the studied eclogite possibly travelled down to the mantle transition zone before it was rapidly carried up by a pre-Mesoproterozoic mantle plume, and subsequently entrained as a xenolith by the Mesoproterozoic (~1.1 Ga) kimberlite.

**1. Introduction**

Subduction of oceanic and/or continental crust into the mantle is one of the most significant processes that control the chemical evolution of the Earth and govern mantle dynamics (Hirose *et al.* 1999; Usui *et al.* 2003). To understand the fate of the subducting crust, i.e. the maximum depth of subduction or evolution and recycling of a subducting crust after slab break-off, especially during Precambrian time, it is essential to study the Precambrian eclogites that formed as a response to the increment of pressure during continued subduction. However, decoding the evolution of the Precambrian subducted crust is challenging owing to the paucity of orogenic/exhumed ultra-high-pressure (UHP) lithologies (eclogites and/or blueschists) in the pre-Mesoproterozoic geological record (e.g. Palin & Santosh, 2021). Kimberlites play an important role as tracers of Precambrian tectonics by directly sampling subduction-related eclogite xenoliths or inclusions in diamonds (e.g. Schmidberger *et al.* 2007; Shirey & Richardson, 2011; Xu *et al.* 2017). Thus, in the absence of orogenic/exhumed eclogites, such subduction-related eclogite xenoliths of pre-Mesoproterozoic age bear significant clues to decode the evolution of subducting crust and mantle dynamics (Jacob, 2004; Aulbach & Jacob, 2016).

The kimberlite-borne eclogite xenoliths, containing UHP minerals that correspond to varying pressures/depths of equilibration, have provided significant details on the evolution and recycling of subducting crust and the dynamics of the sub-continental lithospheric mantle beneath various cratons (e.g. Hills & Haggerty, 1989; Smyth *et al.* 1989; Jacob *et al.* 2003; Jacob, 2004; Shu *et al.* 2016; Mikhailenko *et al.* 2021). For example, an eclogite xenolith containing coesite suggests that the eclogite formed due to subduction (Jacob, 2004) at  $\geq 2.8$  GPa pressure (~100 km depth) (Zhang & Zhang, 2021), whereas the presence of K-rich clinopyroxene and supersilicic or majoritic garnet is indicative of pressure greater than 5 GPa (~175 km depth) (Harlow & Veblen, 1991;

Van Roermund *et al.* 2000). In this study, we deployed *in situ* X-ray diffractometry (XRD), laser Raman spectroscopy and electron probe microanalysis (EPMA) to characterize coesite, majoritic garnet and supersilicic K-rich omphacite in one of the eclogite xenoliths from the Mesoproterozoic (~1.1 Ga) Kalyandurg kimberlite of the Eastern Dharwar Craton, southern India. The geological implications for the presence of such UHP minerals are also discussed in the context of Precambrian mantle geodynamics. Furthermore, we also explore (i) the probable transport mechanism of a subducted slab within the upper mantle for the formation of such UHP minerals, and (ii) how they were brought back to the surface from the mantle transition zone during the Mesoproterozoic kimberlite eruption.

## 2. Geological framework

The Archaean Dharwar Craton of the southern Indian Shield is constituted of two distinct blocks, namely, the Western Dharwar Craton and the Eastern Dharwar Craton that differ on the basis of crustal thickness, lithological associations and grade of metamorphism (Gupta *et al.* 2003; Ramakrishnan & Vaidyanadhan, 2010; Jayananda *et al.* 2018). The Eastern Dharwar Craton is bounded between a steep mylonitic zone in the west, the Chitradurga Shear Zone, and the Proterozoic Eastern Ghats Mobile Belt in the east (Fig. 1a). The craton is a collage of granitoid plutons (Dharwar Batholith) and curvilinear greenstone belts that accreted obliquely to the Western Dharwar Craton during the Neoarchaean (Chadwick *et al.* 2000). The continental crust of the craton is considered to have evolved by accretion during Archaean time in five major episodes (~3.45–3.33 Ga, ~3.23–3.15 Ga, ~3–2.96 Ga, ~2.7–2.6 Ga and ~2.56–2.5 Ga), similar to the other cratons of the globe (Jayananda *et al.* 2020).

Numerous kimberlite pipes are known from the Dharwar Craton and are grouped into the Narayanpet kimberlite field (NKF) in the north, Raichur kimberlite field (RKF) and Tungabhadra kimberlite field (TKF) in the centre and Wajrakarur kimberlite field (WKF) in the south (Fig. 1b). These kimberlites are either of Mesoproterozoic age (~1.1 Ga; Kumar *et al.* 2007; Chalapathi Rao *et al.* 2013; Pandey & Chalapathi Rao, 2020; Dongre *et al.* 2021) or of Late Cretaceous age (~90 Ma; Chalapathi Rao *et al.* 2016). The ~1.1 Ga old WKF is the largest of all these fields and is constituted of different kimberlite clusters: the Wajrakarur, Lattavaram, Chigicherla, Kalyandurg, Timmasamudram and Gooty (Fig. 1b). The oval-shaped kimberlite intrudes the Closepet Granite, which is considered to be a manifestation of late Neoarchaean (~2.5 Ga; Friend & Nutman, 1991) tectonomagmatic activity in the Eastern Dharwar Craton. The present study deals with an eclogite xenolith found in pipe KL-2 of the Kalyandurg cluster, which hosts the largest number of eclogite xenoliths, unlike the other kimberlite pipes of the WKF that are dominated by peridotite xenoliths (Nehru & Reddy, 1989).

The eclogite xenoliths from pipe KL-2 were studied in detail by Patel *et al.* (2006, 2009) and Dongre *et al.* (2015) in terms of their mineralogy, texture and pressure–temperature (*P–T*) evolution. Based on the mineralogy, Patel *et al.* (2006, 2009) classified the eclogites from pipe KL-2 as bimineralic (garnet + omphacite ± rutile), enstatite-bearing (garnet + omphacite + enstatite ± rutile) and celsian-bearing kyanite eclogites (garnet + omphacite + kyanite + celsian ± rutile). In these reports, they inferred the presence of former supersilicic/majoritic garnet. Haggerty & Birkett (2004) and Babu *et al.* (2008) additionally mentioned the presence of coesite in the eclogites of pipe KL-2. However, the proper

identification and undisputed characterization of coesite and majoritic garnet were not established by the previous workers. The *P–T* estimations by Patel *et al.* (2006, 2009) range between 2.8–5 GPa and 800–1225 °C, whereas Dongre *et al.* (2015) calculated the *P–T* as 4.5–5.3 GPa and 1060–1220 °C, which translates to a minimum lithospheric thickness of ~150 km if lithostatic stress is taken into account. Oxygen isotope signatures retrieved from the garnet of eclogites of pipe KL-2 strongly suggest that these eclogites formed owing to subduction (Dongre *et al.* 2015).

## 3. Analytical methods

The *in situ* XRD analysis was carried out at the Inter University Accelerator Centre (IUAC), New Delhi, using a PANalytical EMPYREAN X-ray diffractometer with CuK $\alpha$  radiation ( $\lambda = 1.5406 \text{ \AA}$ ) functioning at 45 kV and 40 mA to identify the minerals from thin-sections. The studied thin-section was scanned at a  $2\theta$  range of 15° to 50° with a step size of 0.02  $\mu\text{m}$  and a count time of 1 second per step. The identified minerals were confirmed by their diffraction patterns from the powder diffraction database of the International Centre for Diffraction Data (ICDD).

Laser Raman analysis and Raman intensity mapping were carried out using a Horiba Jobin Yvon LabRAM HR laser Raman microprobe in the Raman and Fluid Inclusion Laboratory at Wadia Institute of Himalayan Geology, Dehradun. The instrument has a spectral resolution of  $<1 \text{ cm}^{-1}$ . In the present study, a 514 nm laser of argon ion ( $\text{Ar}^+$ ) source was used. Standard silicon was used for calibration, which shows a Raman shift spectrum at  $520.59 \text{ cm}^{-1}$ . Calibration was performed with an error of  $0.1 \text{ cm}^{-1}$ . Accumulations were done for 2 seconds, while the acquisition time was set for 7 to 6 seconds. The grating was fixed at 600 grooves/mm, while the hole width was set as 400  $\mu\text{m}$ . All the measurements were performed under a  $\times 100$  objective lens. Repeated spectra were recorded in the  $200\text{--}700 \text{ cm}^{-1}$  region to obtain better signals for silica polymorphs.

A Horiba Jobin Yvon LabRAM HR Evolution spectrometer installed at the Department of Chemistry, Banaras Hindu University, was also used for laser Raman analysis. The sample was irradiated with the 532 nm laser. Standard silicon was used for calibration, which shows a Raman shift spectrum at  $520.8 \text{ cm}^{-1}$ . Accumulations were carried out for 4 to 10 seconds, and the acquisition time was set for 7 to 15 seconds. The grating was fixed at 1800 grooves/mm, while the hole width was set as 400  $\mu\text{m}$ . All the measurements were performed under a  $\times 100$  objective lens. Repeated spectra were recorded in the  $200\text{--}700 \text{ cm}^{-1}$  region to obtain better signals for quartz and coesite.

Various mineral phases present in the studied xenolith were analysed using a CAMECA-SXFive electron probe microanalyser at the Department of Geology, Banaras Hindu University. Polished thin-sections were coated with a 20 nm carbon layer using a LEICA-EM ACE200 carbon coater prior to the analysis. The instrument was operational at an accelerating voltage of 15 kV and 10 nA current from a LaB $_6$  filament source. Wavelength dispersive X-ray spectrometry in combination with LIF, PET, LPET, TAP and LTAP crystals were used for the quantitative analyses. The diameter of the beam and peak time throughout the analysis were ~1  $\mu\text{m}$  and 10 s, respectively. X-ray intensities were calculated by the X-PHI correction method. Various synthetic and natural reference materials provided by CAMECA-AMETEK were utilized during the calibration.

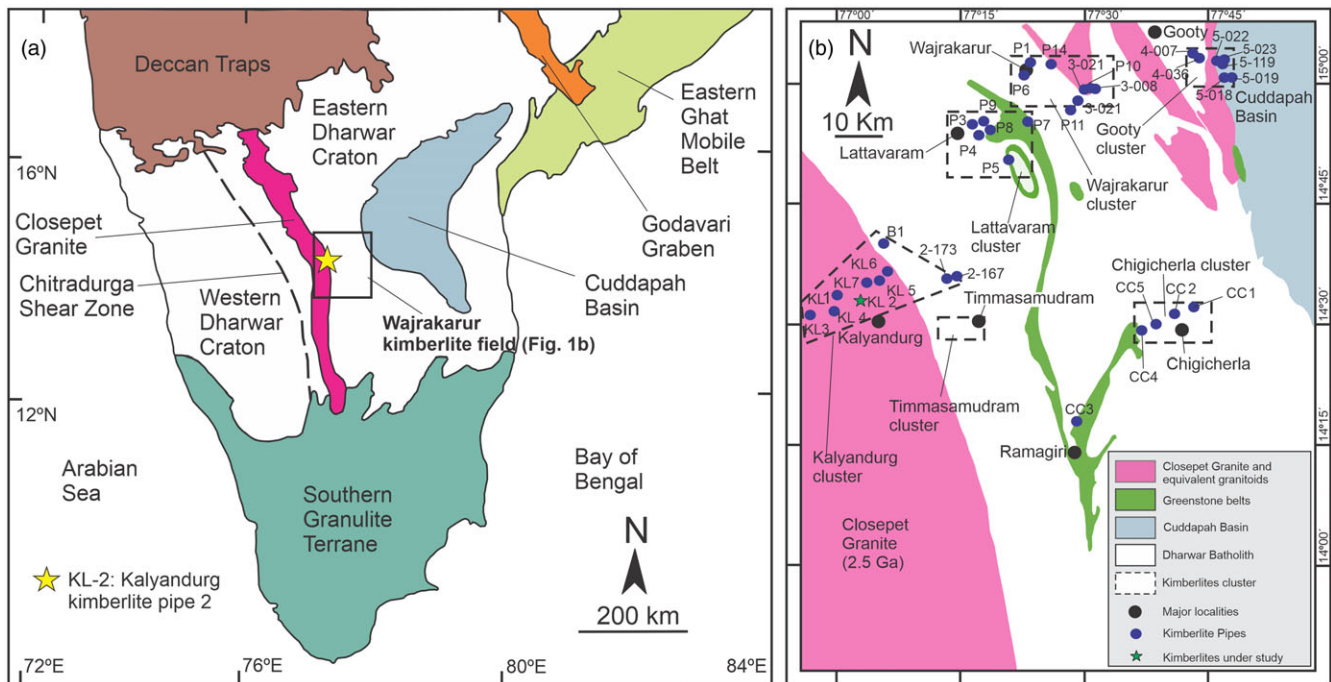


**Fig. 1.** (Colour online) (a) Generalized geological map of peninsular India. (b) Geological map of the Wajrakarur Kimberlite Field in the Eastern Dharwar Craton, India (modified after Nayak & Kudari, 1999; Shaikh *et al.* 2017).

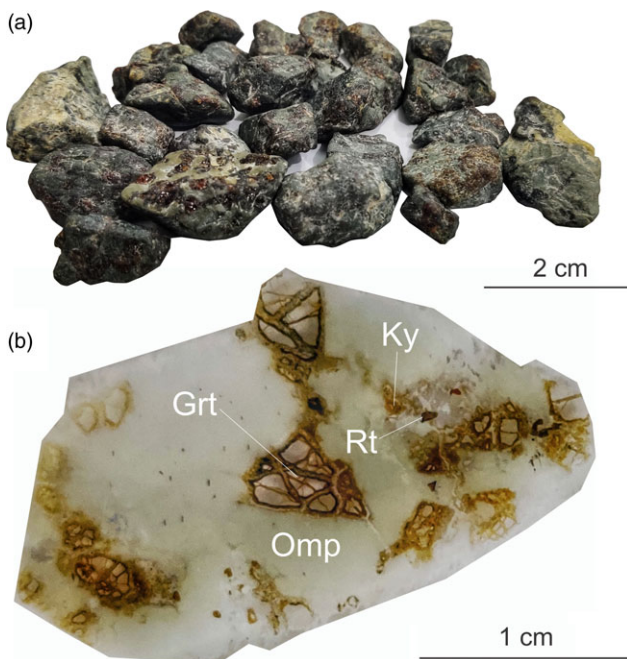


**Fig. 2.** (Colour online) (a) Hand specimens/nodules of eclogite xenoliths collected from the KL-2 kimberlite pipe of the Kalyandurg cluster. (b) Scanned thin-section of the coesite-bearing eclogite sample. Mineral abbreviations: Grt – garnet; Ky – kyanite; Rt – rutile; Omp – omphacite.

## 4. Results

### 4.a. Petrography

A sample from the eclogite xenolith with variable size (6 × 4 cm to 1 × 1 cm) from the KL-2 kimberlite pipe consists of pink-coloured, coarse-grained and rounded to sub-rounded garnet grains

(~400–800 μm in diameter) set in a greyish green to white matrix of altered omphacite. In addition, fine-grained, irregular-shaped majoritic garnet (1000 × 100 μm), kyanite (1200 × 400 μm), quartz/coesite (~50–200 μm in diameter) and rutile were also observed as discrete grains with accessory apatite, barite and chalcopyrite. The whitish appearance of the xenolith is either due to the late-stage alteration or because of interaction between the xenolith and the host kimberlite during ascent (Fig. 2a, b). Coarse-grained garnet is in textural equilibrium with kyanite and quartz/coesite (Fig. 3a, b). These garnet grains are often rimmed by kelyphitic intergrowth of Ca–Al silicate and K-feldspar (Figs 3a, b, 4a, b). Omphacite is fractured and altered. Pristine omphacite compositions are exclusively preserved in the core of altered grains (Fig. 3c). The fine-grained and anisotropic majoritic garnet exclusively occurs along the periphery of the omphacite grains, separating the omphacite from the kelyphitic rim of garnet (Figs 3d, 4c, d). Elongated kyanite grains contain hydrous Ca–Al silicates along the fractures. Quartz/coesite occurs in close association with garnet in the matrix and is often rimmed by polycrystalline quartz (Fig. 4a, b). A curved intragranular deformation fabric is commonly observed within the quartz/coesite (Fig. 3e, f). The quartz/coesite grains are also bleached along the cracks that propagate from the altered matrix similar to that exhibited by omphacite (Figs 3e, f, 4a, b). Rutile is rounded to semi-rounded in shape and often rimmed by ilmenite. Occasionally, rutile is found within the necklace texture that formed at the interface between coarse-grained garnet and omphacite.

### 4.b. Characterization of coesite

Even though the mention of coesite from the eclogites of pipe KL-2 was made before (see Haggerty & Birkett, 2004; Babu *et al.* 2008), no unequivocal supporting evidence from quantitative analytical techniques was provided. Here, a combination of scanning electron microscopy – energy-dispersive X-ray spectroscopy (SEM-EDS),

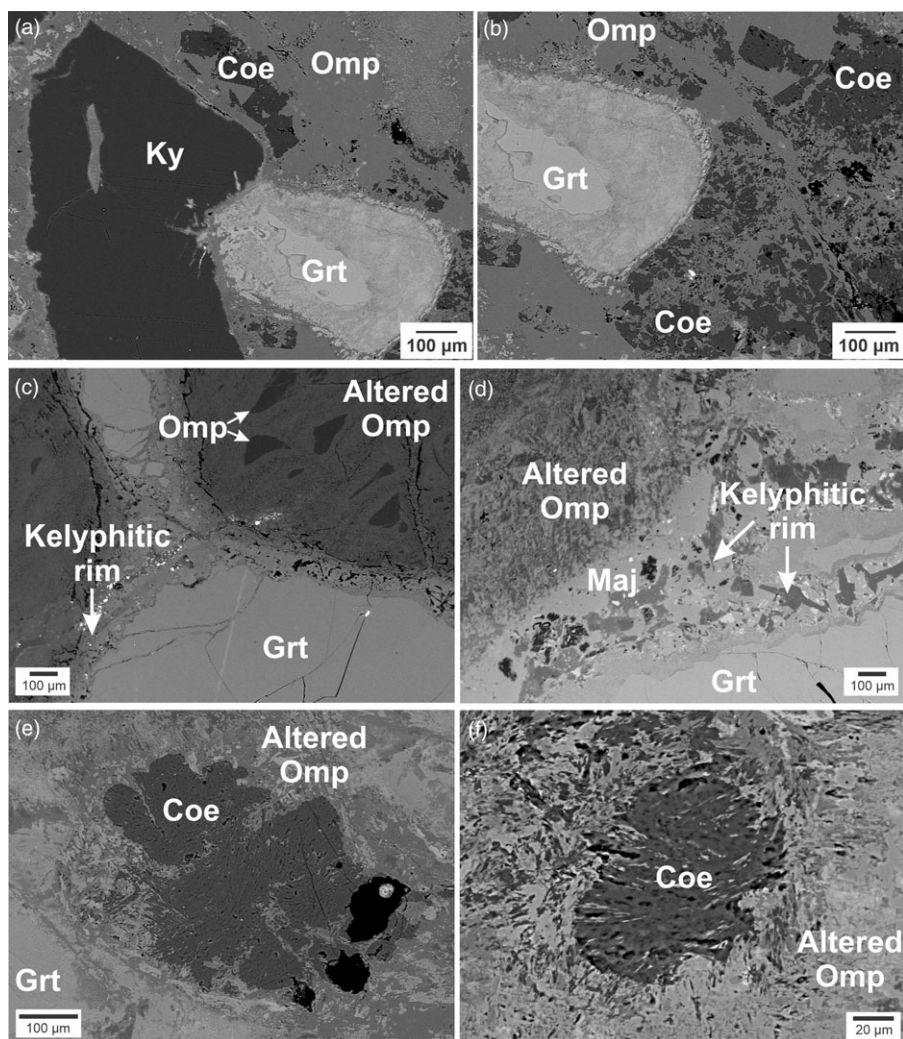


**Fig. 3.** Back-scattered electron (BSE) images of the studied sample depicting (a, b) textural equilibrium of coesite with garnet and kyanite, (c) necklace texture formed at the interface between garnet and clinopyroxene. Fresh omphacite is observed in the core of the altered clinopyroxene. BSE images of (d) the majoritic garnet along the periphery of omphacite, (e, f) different coesite grains found in the matrix. Please note the intra-granular fractures within the grains. Mineral abbreviations: Coe - coesite; Grt - garnet; Ky - kyanite; Maj - majoritic garnet; Omp - omphacite.

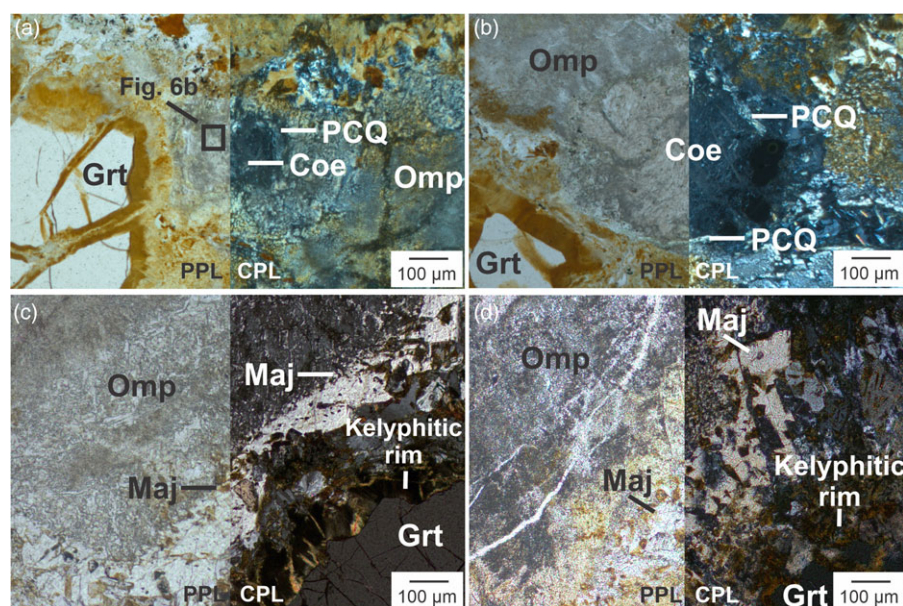


**Fig. 4.** (Colour online) (a, b) Plane- (PPL) and cross-polarized (CPL) photomicrographs showing coesite (Coe) rimmed by polycrystalline quartz (PCQ), along with omphacite (Omp) and garnet (Grt). The black rectangle in (a) marks the location of the Raman intensity map that is shown in Figure 6b. (c, d) PPL and CPL photomicrographs showing the presence of majoritic garnet along the periphery of omphacite. Please note that the majoritic garnet is not isotropic under CPL.

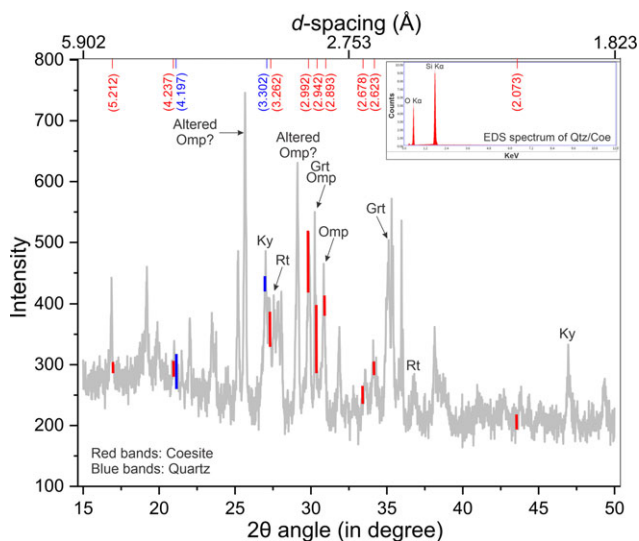


**Fig. 5.** (Colour online) Representative *in situ* XRD spectra of the entire thin-section. The red and blue colour bands are coesite and quartz, respectively. The characteristic XRD spectra of the essential minerals are also marked. The inset figure shows the representative SEM-EDS spectrum of quartz/coesite.

*in situ* XRD and laser Raman spectroscopy coupled with Raman intensity mapping were carried out to characterize the coesite. The initial evidence in favour of quartz/coesite was obtained from SEM-EDS spectra from several grains. A representative EDS spectrum of pure SiO<sub>2</sub> is provided in the inset of Figure 5. To distinguish between quartz and coesite, several transects were chosen across the thin-sections for *in situ* XRD analysis based on the location of quartz/coesite in the sample. The acquired spectra exhibit a collective XRD pattern of all the minerals present. From a representative transect, two characteristic peaks of quartz at 4.197 Å (faint peak with relative intensity = 20.6 %) and 3.302 Å (sharp peak with relative intensity = 100 %; Fig. 5) were identified. The presence of coesite, on the other hand, was confirmed by its nine characteristic peaks (Fig. 5). The characteristic peaks of coesite with higher relative intensity at 3.262 Å (relative intensity = 21.4 %), 2.992 Å (relative intensity = 100 %), 2.942 Å (relative intensity = 19.4 %) and 2.893 Å (relative intensity = 5.1 %) are strong and prominent. Additionally, five characteristic peaks of coesite with lower relative intensity at 5.212 Å (relative intensity = 0.1 %), 4.237 Å (relative intensity = 0.1 %), 2.678 Å (relative intensity = 6.4 %), 2.623 Å (relative intensity = 4.5 %) and 2.073 Å (relative intensity = 1 %) are faint and masked by the background owing to the presence of multiple strong peaks in the vicinity. The characteristic peaks of garnet, kyanite, omphacite and rutile (TiO<sub>2</sub>-I), are also marked in the collective XRD spectra obtained from the representative traverse (Fig. 5).

The characteristic Raman shift spectra of both quartz and coesite were obtained from the unaltered/pristine parts of the targeted grains. The representative monomineralic coesite was identified by the presence of a characteristic sharp peak at 522.3 cm<sup>-1</sup>, with subordinate coesite peaks at 388.05 cm<sup>-1</sup> and 321.1 cm<sup>-1</sup> (Fig. 6a). The presence of monomineralic coesite is further confirmed by Raman intensity mapping. The Raman intensity map for coesite at the 520.8 cm<sup>-1</sup> Raman shift position revealed a strong presence of monomineralic coesite clusters within the representative grain (Figs 4a, 6b). The representative bimineralic quartz and coesite were characterized by a sharp and symmetric Raman shift spectra at 462.7 cm<sup>-1</sup> (quartz) and 518.4 cm<sup>-1</sup> (coesite), with minor peaks

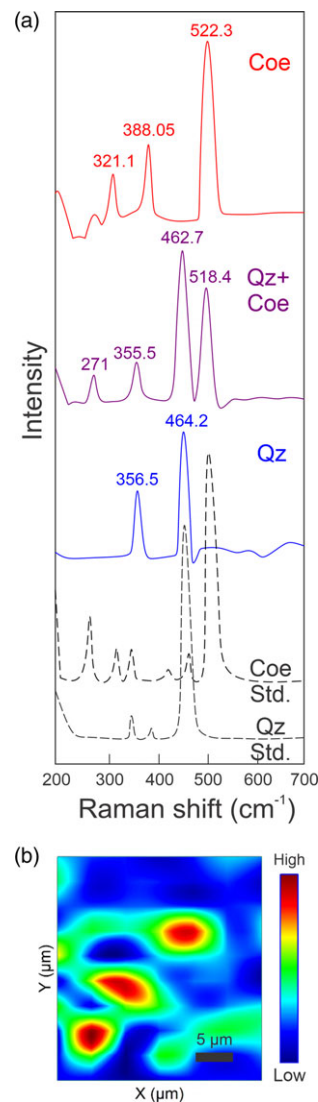


**Fig. 6.** (Colour online) (a) Representative laser Raman spectra of the monomineralic coesite (522.3, 388.05 and 321.1 cm<sup>-1</sup>; red), bimineralic quartz + coesite (quartz: 462.7 and 355.5 cm<sup>-1</sup>; coesite: 518.4 and 271.1 cm<sup>-1</sup>; purple) and monomineralic quartz (464.2 and 356.5 cm<sup>-1</sup>; blue), respectively. The standard spectra of quartz and coesite from the Ruff database is also provided for reference. (b) Representative Raman intensity map of a coesite/quartz grain showing the strong presence of coesite as a cluster.

of quartz and coesite at 355.5 cm<sup>-1</sup> and 271.0 cm<sup>-1</sup>, respectively (Fig. 6a). A strong representative Raman shift peak at 464.2 cm<sup>-1</sup> with a subordinate peak at 356.5 cm<sup>-1</sup> confirmed the presence of monomineralic quartz (Fig. 6a) that occurs mostly along the rim of the grain. Occasionally, patches of bimineralic quartz + coesite and monomineralic quartz are randomly distributed adjacent to the monomineralic coesite, without forming any core–mantle–rim structure of coesite, quartz + coesite and quartz.

#### 4.c. Characterization of coarse-grained and majoritic garnet

The composition of the coarse-grained and rounded to sub-rounded garnet cores is represented by Alm<sub>38–41</sub>Prp<sub>14–15</sub>Grs<sub>44–47</sub>Sps<sub>0–1</sub> with X<sub>Fe</sub> ranging between 0.72 and 0.74 (Table 1). The Si atoms per formula unit (apfu) range from 2.90 to 3.02 (Table 1; Fig. 7). Except for one point with Si apfu of 3.02, such garnet grains are completely devoid of Na (Table 1). There is

**Table 1.** EPMA mineral chemical data of garnet core

Sample	KL-2C	KL-2C	KL-2C	KL-2C	KL-2C	KL-2C	KL-2C	KL-2C	KL-2C	KL-2C
SiO <sub>2</sub>	38.48	38.49	38.65	38.44	39.21	37.20	37.20	38.33	38.49	38.68
TiO <sub>2</sub>	0.37	0.34	0.40	0.34	0.28	0.38	0.36	0.32	0.35	0.39
Al <sub>2</sub> O <sub>3</sub>	21.05	21.13	21.43	21.24	21.45	21.45	21.35	21.35	21.37	21.48
Cr <sub>2</sub> O <sub>3</sub>	0.04	0.09	0.06	n.d.	0.14	n.d.	0.06	n.d.	0.10	0.03
FeO	18.62	18.32	18.96	19.40	17.17	19.88	18.88	18.53	18.24	19.53
MnO	0.23	0.19	0.37	0.15	0.20	0.23	0.31	0.28	0.20	0.28
MgO	3.81	3.80	3.77	3.78	3.82	4.04	3.97	4.01	3.94	3.93
CaO	16.58	16.30	16.63	16.20	16.18	16.81	16.37	16.54	16.34	16.23
Na <sub>2</sub> O	n.d.	n.d.	n.d.	n.d.	1.25	n.d.	n.d.	n.d.	n.d.	n.d.
K <sub>2</sub> O	0.02	0.02	0.08	0.09	n.d.	n.d.	n.d.	n.d.	n.d.	n.d.
Total	99.20	98.69	100.36	99.65	99.70	99.98	98.49	99.36	99.03	100.55
Si	3.00	3.01	2.98	2.99	3.02	2.90	2.93	2.98	3.00	2.98
Ti	0.02	0.02	0.02	0.02	0.02	0.02	0.02	0.02	0.02	0.02
Al	1.93	1.95	1.95	1.95	1.95	1.97	1.98	1.96	1.96	1.95
Cr	0.00	0.01	0.00	0.00	0.01	0.00	0.00	0.00	0.01	0.00
Fe <sup>2+</sup>	1.21	1.20	1.22	1.26	1.11	1.30	1.24	1.21	1.19	1.26
Mn	0.01	0.01	0.02	0.01	0.01	0.01	0.02	0.02	0.01	0.02
Mg	0.44	0.44	0.43	0.44	0.44	0.47	0.47	0.46	0.46	0.45
Ca	1.38	1.36	1.37	1.35	1.34	1.41	1.38	1.38	1.36	1.34
Na	0.00	0.00	0.00	0.00	0.19	0.00	0.00	0.00	0.00	0.00
K	0.00	0.00	0.01	0.01	0.00	0.00	0.00	0.00	0.00	0.00
Total	8.01	8.00	8.02	8.02	8.08	8.09	8.05	8.02	8.00	8.02
Garnet end-members										
X <sub>Prp</sub>	0.14	0.15	0.14	0.14	0.15	0.15	0.15	0.15	0.15	0.15
X <sub>Alm</sub>	0.40	0.40	0.40	0.41	0.38	0.41	0.40	0.39	0.39	0.41
X <sub>Grs</sub>	0.45	0.45	0.45	0.44	0.46	0.44	0.44	0.45	0.45	0.44
X <sub>Sps</sub>	0.00	0.00	0.01	0.00	0.00	0.00	0.01	0.01	0.00	0.01

n.d = not detected.

X<sub>Prp</sub> = (Mg/(Fe<sup>2+</sup> + Mg + Ca + Mn)), X<sub>Alm</sub> = (Fe<sup>2+</sup>/(Fe<sup>2+</sup> + Mg + Ca + Mn)), X<sub>Grs</sub> = (Ca/(Fe<sup>2+</sup> + Mg + Ca + Mn)), X<sub>Sps</sub> = (Mn/(Fe<sup>2+</sup> + Mg + Ca + Mn)).

Peak T<sup>a</sup> = 1579–1119 °C, Peak T<sup>b</sup> = 1478–1085 °C.

Peak P<sup>a</sup> = 8–5 GPa, Peak P<sup>c</sup> = 7–5 GPa.

a = using Krogh Ravna & Terry (2004).

b = using Ellis & Green (1979).

c = P calculated using T estimated by Ellis & Green (1979) projected on the steady-state geotherm of the Kalyandurg cluster taken from Karmalkar *et al.* (2009).

another group of compositionally and texturally distinct garnet with high silica content (Si apfu = 3.18–3.61) (Table 2; Fig. 7). The Na<sub>2</sub>O and CaO contents in these fine-grained and irregular-shaped garnets vary from 0.48 to 1.60 wt % and 19.64 to 21.47 wt %, respectively (Table 2), which is higher than that in the garnet with Si apfu 2.90–3.02. Considering the Si apfu ≥ 3.05 as a threshold value for the characterization of supersilicic or majoritic garnet (Tappert *et al.* 2005), these high Si–Na–Ca garnet are classified as majoritic garnets (Fig. 7).

Evidence in support of majoritic garnet comes from the laser Raman shift spectra (Fig. 8). The broad peaks between 800 and 900 cm<sup>-1</sup> obtained from inclusion-free majoritic garnet are the characteristic Raman shift spectra for majoritic garnet (Fig. 8), which indicate the presence of excess Si in the octahedral site

(Gillet *et al.* 2002; Kunz *et al.* 2002), along with the characteristic sharp peaks at 911.5 and 913.2 cm<sup>-1</sup> (Kunz *et al.* 2002; Stähle *et al.* 2011). Compared with the global dataset of majoritic garnet, the composition of the majoritic garnet in this study is unique in terms of high Ca and low Mg content. Hence, it is difficult to compare the obtained Raman shift spectra with published data. However, we compared our Raman shift spectra with the Raman shift spectra of Hofmeister *et al.* (2004) and Stähle *et al.* (2011) because of the nearly identical Si apfu. The Raman shift spectra at 549.1, 566.5, 661.8 and 663.6 cm<sup>-1</sup> for majoritic garnet with Si apfu 3.39 of Hofmeister *et al.* (2004) and Stähle *et al.* (2011) are matched with the Raman shift spectra obtained in this study. The subordinate peaks at 347.8, 379.9, 549.1, 1013 and 1014.6 cm<sup>-1</sup> correspond well with the Raman spectra of the omphacite (Fig. 8).

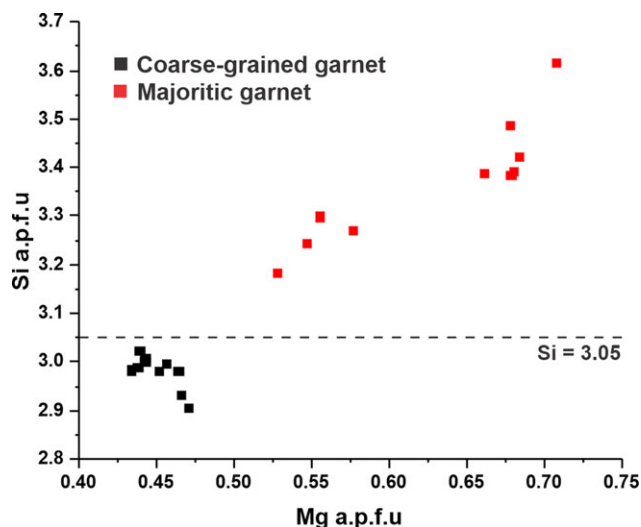


**Fig. 7.** (Colour online) A Si apfu versus Mg apfu plot of the garnet and majoritic garnet from the studied sample. The Si = 3.05 line demarcates the coarse-grained garnet from majoritic garnet.

#### 4.d. Mineral chemistry of K-omphacite

Since the clinopyroxenes are highly altered, the composition of their rims could not be determined. The cores of clinopyroxene, which are devoid of any intergrowth/inclusions (Fig. 3c), are omphacitic with Na<sub>2</sub>O ranging between 3.97 and 5.87 wt % (Table 3). Interestingly, these omphacites are supersilicic (Si > 2 apfu; Table 3) with a negligible Ca-Tschermakite component. In addition, the omphacites are rich in Al<sub>2</sub>O<sub>3</sub> (16.98–19.53 wt %) and K<sub>2</sub>O (0.73–2.94 wt %, average = 1.78 ± 0.21 wt %) (Table 3; Fig. 9).

#### 4.e. Geothermobarometry

Two conventional geothermobarometers were used to constrain the maximum *P*–*T* conditions under which the coarse-grained garnet–clinopyroxene–kyanite–rutile–coesite assemblage evolved. Sobolev *et al.* (1999) observed that Fe<sup>3+</sup>/total Fe has a compensation effect on garnet and clinopyroxene, which, in turn, does not change actual temperature estimates of the eclogites. Thus, the Fe<sup>2+</sup> of garnet and clinopyroxene was considered as total Fe for the Mg–Fe<sup>2+</sup> exchange geothermometer of Ellis & Green (1979). On the other hand, the garnet–clinopyroxene–kyanite–coesite ± phengite net-transfer geothermobarometer of Krogh Ravna & Terry (2004) is not effected by the Fe<sup>3+</sup>/total Fe estimation (Krogh Ravna & Paquin, 2003). Owing to the presence of excess silica (>2 apfu), the Al<sup>IV</sup> in T site could not be calculated (Al<sup>IV</sup> = 2–Si) for clinopyroxene, which barred the use of the garnet–clinopyroxene geobarometer of Beyer *et al.* (2015).

Application of the qualitative K-in-pyroxene barometer of Safonov *et al.* (2005) estimates a pressure of between 6 and 7 GPa (Fig. 10). The core compositions of coarse-grained garnet and clinopyroxene were used for the garnet–clinopyroxene geothermometer of Ellis & Green (1979). The temperature estimation ranges between 1085 and 1478 °C (Table 1). Considering the temperature range, the pressure is calculated as ~5–7 GPa by projecting the temperature on the steady-state geotherm of the Kalyandurg cluster during the xenolith entrapment in Mesoproterozoic time (reviewed in Karmalkar *et al.* 2009). The projected pressure is higher than the value of Patel *et al.* (2006,

2009) and Dongre *et al.* (2015) owing to the increment of temperature estimation. The unambiguous characterization of coesite for the first time from the Kalyandurg cluster enabled us to use the garnet–clinopyroxene–kyanite–coesite ± phengite geothermobarometer of Krogh Ravna & Terry (2004). The temperature estimation ranged between 1119 and 1579 °C, whereas the pressure was computed as ~5–8 GPa (Fig. 11a; Table 1).

To constrain the pressure of formation of the majoritic garnets, single-mineral geobarometers based on the Si content of majoritic garnet were used. The formation pressure of majoritic garnet ranges between 9.4 and 17 GPa (after Tao *et al.* 2018), 9.3 and 17 GPa (after Collerson *et al.* 2010), 10.7 and 22.6 GPa (after Wijbrans *et al.* 2016) and 7.7 and 16 GPa (after Beyer & Frost, 2017).

## 5. Discussion

The mineralogy of the studied sample is unique for the kimberlite-borne eclogite xenoliths from the Eastern Dharwar Craton as it contains a plethora of UHP minerals such as coesite, K-omphacite and majoritic garnet along with coarse-grained garnet, kyanite and rutile. However, a similar mineralogical assemblage has been reported from the kimberlite-derived eclogite xenoliths from the (i) Kaapvaal craton (e.g. Viljoen, 1995; Jacob *et al.* 2003; Schmickler *et al.* 2004; Shu *et al.* 2016), (ii) the West African craton (e.g. Hills & Haggerty, 1989) and (iii) the Siberian craton (e.g. Alifirova *et al.* 2015; Mikhailenko *et al.* 2020). In the following sections, we will discuss the possible implications of the presence of such UHP minerals.

### 5.a. Implication of coesite

The kimberlite-borne eclogite xenoliths are known to have formed either by subduction of oceanic crust or tectonic emplacement of oceanic crustal cumulates into the mantle (Jacob, 2004; Aulbach & Arndt, 2019). Coesite-bearing eclogites can only form by the subduction of crust at a depth of more than 100 km, and the presence of free silica rules out their origin as high-pressure cumulates (Schulze *et al.* 2000; Jacob, 2004). A high-pressure cumulate origin of mantle eclogites is also not consistent with their geochemistry (see Aulbach & Jacob 2016; Aulbach & Arndt, 2019). The subduction-related origin of the kimberlite-borne eclogite xenoliths from the Kalyandurg cluster is well established based on δ<sup>18</sup>O in garnet restricted between +5.3 ‰ and +7.8 ‰ (Dongre *et al.* 2015). A heavy Li isotope signature (δ<sup>7</sup>Li up to 9.7 ‰) similar to an ancient altered oceanic crust is also observed in the mantle sources of the Wajrakarur kimberlites (Krmíček *et al.* 2022). This study revealed the presence of coesite, which is the first mineralogical evidence in favour of the subduction of oceanic crust of the Dharwar craton, at least, up to ~100 km.

The presence of monomineralic quartz and bimineralic quartz + coesite (Fig. 6a) along with intragranular fracture (Fig. 4a, b) implies complete to partial transformation of coesite to quartz during depressurization vis-à-vis volume expansion. Since the coesite to quartz transformation is energetically less favourable than the quartz ⇌ coesite, the conversion of coesite to quartz is more common in coesite-bearing ‘orogenic’ eclogites (e.g. Ye *et al.* 2001; Perrillat *et al.* 2003; Gonzalez *et al.* 2020) owing to their prolonged exhumation history. In contrast, kimberlite-derived coesite-bearing eclogite xenoliths experience rapid ascension from the mantle to the crust (Kelley & Wartho, 2000), which helped to preserve the coesite. However, the formation of quartz after coesite is reported from various kimberlite-derived coesite-bearing

**Table 2.** EPMA mineral chemical data of majoritic garnet

Sample	KL-2C	KL-2C	KL-2C	KL-2C	KL-2C	KL-2C	KL-2C	KL-2C	KL-2C	KL-2C
SiO <sub>2</sub>	42.34	46.01	44.73	41.14	43.89	41.54	42.54	43.26	43.20	43.21
TiO <sub>2</sub>	0.64	0.40	0.43	0.52	0.36	0.70	0.64	0.55	0.54	0.55
Al <sub>2</sub> O <sub>3</sub>	15.32	8.33	11.12	17.50	12.27	15.15	14.15	11.25	11.64	11.83
Cr <sub>2</sub> O <sub>3</sub>	0.03	0.03	0.06	0.10	0.00	0.07	0.07	0.06	0.09	0.06
FeO	13.61	16.37	15.12	13.09	14.79	15.00	16.10	16.51	15.28	17.03
MnO	0.14	0.18	0.17	0.11	0.25	0.18	0.13	0.27	0.29	0.12
MgO	5.01	6.04	5.83	4.58	5.89	4.70	4.80	5.67	5.81	5.81
CaO	21.32	20.52	20.60	20.95	20.51	20.89	20.73	20.50	21.47	19.64
Na <sub>2</sub> O	0.85	0.59	0.62	0.74	0.63	0.61	0.71	1.60	0.62	0.48
K <sub>2</sub> O	0.01	0.00	0.00	0.02	0.00	0.01	0.00	0.03	0.01	0.32
Total	99.28	98.47	98.68	98.74	98.60	98.84	99.87	99.69	98.95	99.05
Cations for 12 oxygen atoms										
Si	3.27	3.61	3.49	3.18	3.42	3.24	3.30	3.39	3.38	3.39
Ti	0.04	0.02	0.03	0.03	0.02	0.04	0.04	0.03	0.03	0.03
Al	1.39	0.77	1.02	1.60	1.13	1.39	1.29	1.04	1.07	1.09
Cr	0.00	0.00	0.00	0.01	0.00	0.00	0.00	0.00	0.01	0.00
Fe <sup>2+</sup>	0.88	1.08	0.99	0.85	0.96	0.98	1.04	1.08	1.00	1.12
Mn	0.01	0.01	0.01	0.01	0.02	0.01	0.01	0.02	0.02	0.01
Mg	0.58	0.71	0.68	0.53	0.68	0.55	0.55	0.66	0.68	0.68
Ca	1.76	1.73	1.72	1.74	1.71	1.75	1.72	1.72	1.80	1.65
Na	0.13	0.09	0.09	0.11	0.10	0.09	0.11	0.24	0.09	0.07
K	0.00	0.00	0.00	0.00	0.00	0.00	0.00	0.00	0.00	0.03
Total	7.93	7.93	7.93	7.93	7.95	7.97	7.96	7.94	8.00	7.98
Estimated pressure (in GPa)										
P <sup>1</sup>	11.3	17.0	14.7	9.4	13.7	11.3	12.0	14.5	14.2	14.0
P <sup>2</sup>	11.0	17.0	14.6	9.3	13.6	10.7	12.0	13.7	13.5	13.4
P <sup>3</sup>	13.1	22.6	19.1	10.7	17.3	12.4	14.0	16.4	16.3	16.5
P <sup>4</sup>	9.6	16.0	13.8	7.7	12.7	9.1	10.0	12.0	11.9	12.1

Pressure estimated using the following barometers: 1 – Tao *et al.* (2018); 2 – Collerson *et al.* (2010); 3 – Wijbrans *et al.* (2016); 4 – Beyer & Frost (2017).

eclogite xenoliths (Schulze & Helmstaedt, 1988; Schmickler *et al.* 2004; Mikhailenko *et al.* 2021). Such coesite  $\rightleftharpoons$  quartz transformation is energetically favourable if the phase transition during depressurization occurs at a temperature  $>800$  °C (Zhong *et al.* 2018). The coesite-bearing eclogite xenolith of the present study has been hosted in a kimberlite magma hotter than 800 °C (Kavanagh & Sparks, 2009) that may have facilitated partial transformation to quartz from coesite. The preservation of coesite is also dependent on the low H<sub>2</sub>O content (Mosenfelder *et al.* 2005). The absence altogether of hydrous minerals, such as mica and amphibole, suggests the concentration of H<sub>2</sub>O was low in our sample, which helped to preserve the coesite. The presence of coesite in the eclogite xenolith undisputedly reveals an equilibration deeper than 100 km in the upper mantle.

### 5.b. Implication of K-omphacite

The pristine cores of the clinopyroxenes of the studied sample revealed that they are potassium-rich omphacites. Potassium-rich

clinopyroxenes/omphacites are exclusively found as inclusions in diamond (Safonov *et al.* 2011); however, anomalously higher K<sub>2</sub>O (3.61 wt %) in natural samples, comparable to those from the present study, are only reported from Kumdy-Kol diamond mine in Kokchetav Complex, Kazakhstan (Bindi *et al.* 2003; Fig. 9). In supersilicic clinopyroxenes, the excess silica is accommodated at the M1 octahedral site (Angel *et al.* 1988; Day & Mulcahy, 2007). Experimental and natural system investigations have demonstrated that the formation of supersilicic clinopyroxene requires UHP conditions and temperatures exceeding 1100 °C (Katayama *et al.* 2000; Okamoto *et al.* 2000). This is consistent with the absence of phengite in the matrix, which is unstable at temperatures above 950 °C (Okamoto *et al.* 2000). Although K-enrichment in clinopyroxene is generally attributed to diamond-forming UHP conditions ( $>5$  GPa), it can also be formed in an unusual K-rich environment resulting from metasomatism by potassic melts (Navon *et al.* 1988; Harlow & Veblen, 1991). The absence of K-rich phases such as phlogopite, K-richterite and K–Ba-titanite ubiquitous in potassic melt-induced modal metasomatism (Safonov *et al.*



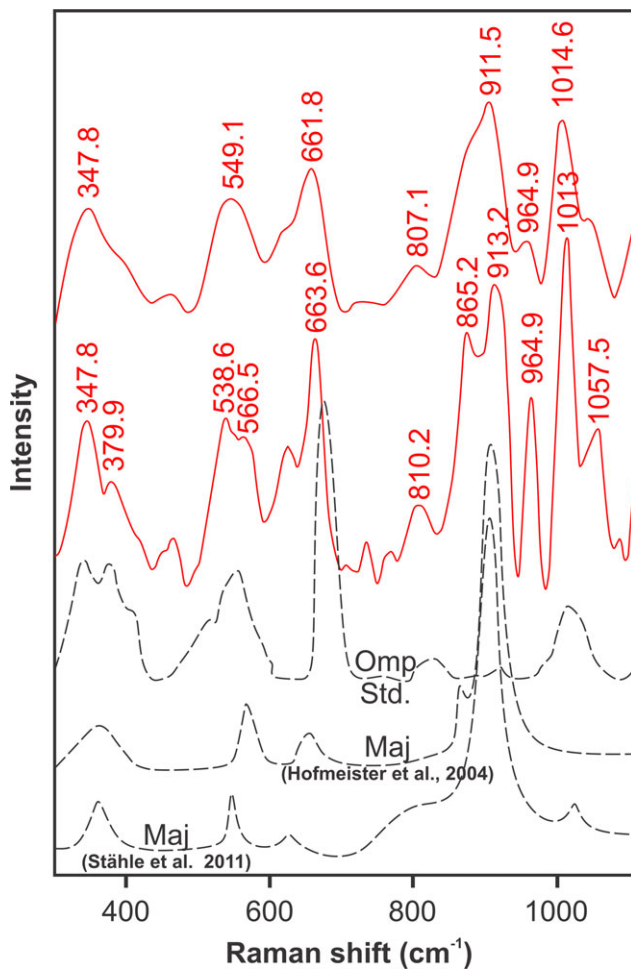


**Fig. 8.** (Colour online) Representative laser Raman spectra of the majoritic garnet (red) along with the standard Raman spectra of omphacite (Ruff database) and majoritic garnet of Hofmeister *et al.* (2004) and Stähle *et al.* (2011), which have identical Si apfu compared to the studied sample.

2019) is not consistent with a metasomatism-induced K-enrichment in clinopyroxene in the present case, although the role of cryptic metasomatism cannot be entirely ruled out in the absence of trace-element data.

The  $P$ - $T$  estimations involving coarse-grained garnet and K-omphacite along with kyanite and coesite suggest that they were equilibrated at  $\sim 5$ – $8$  GPa and  $\sim 1085$ – $1579$  °C. Application of the qualitative K-in-pyroxene barometer estimates the pressure between 6 and 7 GPa (Fig. 10). Since K-feldspar in a subducting crust is unstable at  $>5$  GPa, the formation of K-clinopyroxene and coesite at such UHP conditions is explained by the breakdown of K-feldspar into K-clinopyroxene + coesite (Okamoto *et al.* 2000). Hence, by combining the  $P$ - $T$  estimations of different geothermobarometers, we suggest that the garnet–clinopyroxene (K-omphacite)–kyanite–coesite assemblage of our sample equilibrated at  $\sim 5$ – $8$  GPa and  $\sim 1085$ – $1579$  °C. Compared to the maximum pressure estimations of 5–5.5 GPa by Patel *et al.* (2006, 2009) and Dongre *et al.* (2015), this is the highest pressure estimated so far from the xenoliths of the Kalyandurg cluster (Fig. 11a). Our pressure estimation corresponds to a lithospheric thickness of  $\sim 175$ – $280$  km and implies that there was a very thick cratonic root with a wide diamond stability window during the kimberlite magmatism at  $\sim 1.1$  Ga.

### 5.c. Implication of majoritic garnet

The studied sample contains fine-grained, Ca-rich majoritic garnet at the periphery of K-omphacite and coarse-grained garnet (Figs 3d, 4c, d). According to the textural relationship between the majoritic garnet, K-omphacite and coarse-grained garnet, it is observed that the majoritic garnet and kelyphitic rim separates K-omphacite from the coarse-grained garnet (Figs 3d, 4c, d), which suggests that the majoritic garnet, along with the kelyphitic rim, formed via reaction between coarse-grained garnet and K-omphacite. The formation of Ca-majorite as a dissociated product of diopside has been already established based on the presence of overlapping peaks between Ca-majorite and diopside (Tomioka & Kimura, 2003; Ghosh *et al.* 2021). The presence of weak anisotropy as observed under the optical microscope (Fig. 4c, d) suggests the absence of cubic symmetry of the majoritic garnet. Such an absence of cubic symmetry is possible either (i) owing to the partial or incomplete transformation from omphacite to majoritic garnet (Xie & Sharp, 2007) or (ii) by a symmetry reduction from cubic to tetragonal through Mg–Si ordering in the octahedral sites upon cooling (Hatch & Ghose, 1989; Tomioka *et al.* 2002). The textural relationship between the majoritic garnet, coarse-grained garnet and omphacite coupled with the overlapping Raman spectra between the majoritic garnet and omphacite strongly suggests that the studied majoritic garnet formed owing to dissociation of coarse-grained garnet and omphacite with increasing pressure, which also explains the presence of excess  $\text{Na}_2\text{O}$  and CaO in such majoritic garnet.

The majoritic garnets are a stable phase at pressures  $>5$  GPa (Van Roermund *et al.* 2000) and are reported from the eclogite xenoliths of other Kalyandurg cluster kimberlites (Pipe P3; Patel *et al.* 2009). Dissolution of the pyroxene component in the garnet structure with increasing pressure/depth causes four-fold tetrahedral coordination of Si to be converted into six-fold octahedral coordination (Akaogi & Akimoto, 1977; Irifune, 1987). The presence of Si at the octahedral site in garnet is achieved by (i) the replacement of a trivalent cation ( $\text{Al}^{3+}$  and  $\text{Cr}^{3+}$ ) of octahedral coordination by a divalent cation ( $\text{Mg}^{2+}$ ,  $\text{Ca}^{2+}$ ,  $\text{Fe}^{2+}$ ) and  $\text{Si}^{4+}$  leading to its supersilicic nature, (ii) Al deficiency and (iii) an increased majoritic component represented by  $^{\text{viii}}\text{M}_3^{\text{vi}}(\text{Al}_{2-2n}\text{M}_n\text{Si}_n)^{\text{iv}}\text{Si}_3\text{O}_{12}$ , where  $M$  is a divalent cation and  $n$  ranges between 0 and 1 (Akaogi & Akimoto, 1977; Moore & Gurney, 1985; Irifune, 1987). Majoritic garnets are rare in mantle xenoliths, unlike the inclusions in diamonds, but are known from many kimberlite-borne mantle xenoliths (Haggerty & Sautter, 1990; Sautter *et al.* 1991; Doukhan *et al.* 1994; Roermund & Drury, 1998; Xu *et al.* 2017). The studied majoritic garnet is rich in CaO unlike the MgO-rich majoritic garnet found in other eclogite xenoliths and diamond inclusions (see Thompson *et al.* 2021).

A high  $\text{Na}_2\text{O}$  in the majoritic garnets points to a high-pressure origin ( $>6$  GPa) corresponding to  $>200$  km depth, well within the diamond stability field (Sobolev, 1977; Ye *et al.* 2001). To constrain the pressure of formation of these majoritic garnets, several single-mineral geobarometers were used. The pressure ranges between (i) 9.4 and 17 GPa (after Tao *et al.* 2018), (ii) 9.3 and 17 GPa (after Collerson *et al.* 2010), (iii) 10.7 and 22.6 GPa (after Wijbrans *et al.* 2016) and (iv) 7.7 and 16 GPa (after Beyer & Frost, 2017), all of which correspond to a depth range of 280–660 km, up to the base of the upper mantle or mantle transition zone.

The presence of kimberlite-borne eclogite xenoliths confirms the existence of an eclogite reservoir in the lithospheric mantle beneath the Eastern Dharwar Craton, which is a more fertile source

**Table 3.** EPMA mineral chemical data of K-omphacite

Sample	KL-2C	KL-2C	KL-2C	KL-2C	KL-2C	KL-2C	KL-2C	KL-2C	KL-2C	KL-2C
SiO <sub>2</sub>	58.81	59.21	58.79	58.89	59.06	55.28	58.83	57.60	55.62	57.91
TiO <sub>2</sub>	0.36	0.25	0.26	0.24	0.25	0.25	0.36	0.17	0.40	0.29
Al <sub>2</sub> O <sub>3</sub>	17.22	17.75	17.37	18.13	19.53	17.86	16.98	19.21	17.69	18.20
Cr <sub>2</sub> O <sub>3</sub>	n.d.	0.02	0.02	0.05	n.d.	n.d.	0.14	n.d.	0.16	0.16
FeO	3.08	3.65	3.15	3.00	3.02	4.88	3.07	3.74	4.50	3.97
MnO	0.07	n.d.	n.d.	n.d.	n.d.	0.15	n.d.	0.05	0.08	0.03
MgO	3.01	2.13	3.20	2.38	2.45	3.66	3.98	4.11	4.09	3.43
CaO	9.39	8.90	8.83	8.93	7.47	10.72	9.24	8.40	11.26	11.40
Na <sub>2</sub> O	5.84	5.87	4.84	5.74	4.80	4.50	5.25	3.97	4.21	4.62
K <sub>2</sub> O	1.76	1.75	2.94	1.96	2.14	2.38	0.73	1.74	1.59	0.84
Total	99.54	99.54	99.40	99.33	98.71	99.68	98.59	99.01	99.58	100.84
Cations for 6 oxygen atoms										
Si	2.045	2.056	2.049	2.046	2.046	1.956	2.048	2.001	1.959	1.993
Ti	0.009	0.007	0.007	0.006	0.007	0.007	0.009	0.005	0.011	0.008
Al	0.706	0.727	0.713	0.742	0.797	0.745	0.697	0.787	0.734	0.738
Cr	0.000	0.000	0.000	0.001	0.000	0.000	0.004	0.000	0.004	0.004
Fe <sup>2+</sup>	0.090	0.106	0.092	0.087	0.087	0.145	0.089	0.109	0.132	0.114
Mn	0.002	0.000	0.000	0.000	0.000	0.004	0.000	0.002	0.002	0.001
Mg	0.156	0.110	0.166	0.123	0.126	0.193	0.207	0.213	0.215	0.176
Ca	0.350	0.331	0.330	0.333	0.277	0.407	0.344	0.313	0.425	0.420
Na	0.394	0.396	0.327	0.387	0.323	0.309	0.355	0.268	0.287	0.308
K	0.078	0.077	0.131	0.087	0.095	0.107	0.033	0.077	0.071	0.037
Total	3.829	3.810	3.816	3.813	3.758	3.872	3.786	3.773	3.841	3.800

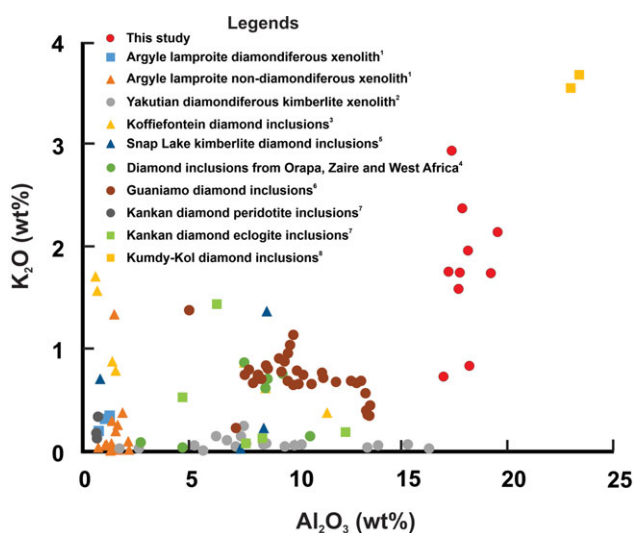


**Fig. 9.** (Colour online) K<sub>2</sub>O-in-Cpx versus Al<sub>2</sub>O<sub>3</sub>-in-Cpx plot of various diamond-hosted clinopyroxene found in the xenoliths. Please note that the clinopyroxene of this study contains one of the highest amounts of Al<sub>2</sub>O<sub>3</sub> and K<sub>2</sub>O. Data sources are: 1 – Jaques *et al.* (1990); 2 – Snyder *et al.* (1997); 3 – Harlow (1997); 4 – Prinz *et al.* (1975); 5 – Pokhilenko *et al.* (2004); 6 – Kaminsky *et al.* (2000); 7 – Stachel *et al.* (2000); 8 – Bindi *et al.* (2003).

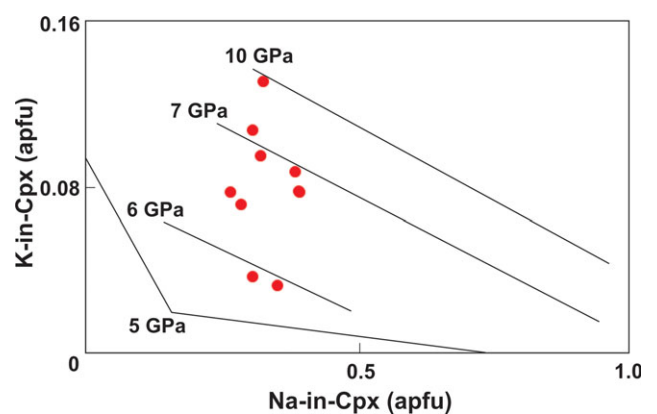


**Fig. 10.** (Colour online) K-in-Cpx versus Na-in-Cpx plot (after Safonov *et al.* 2005) showing that the pressure of our sample is mostly constrained between 6 and 7 GPa.

for diamond than mantle peridotites (Stachel & Harris, 2008). Furthermore, a plethora of UHP minerals (coesite, K-omphacite and majoritic garnet) that formed between ~175 and 660 km preserved in the studied eclogite xenolith point to a viable diamond prospect in the Kalyandurg kimberlites.

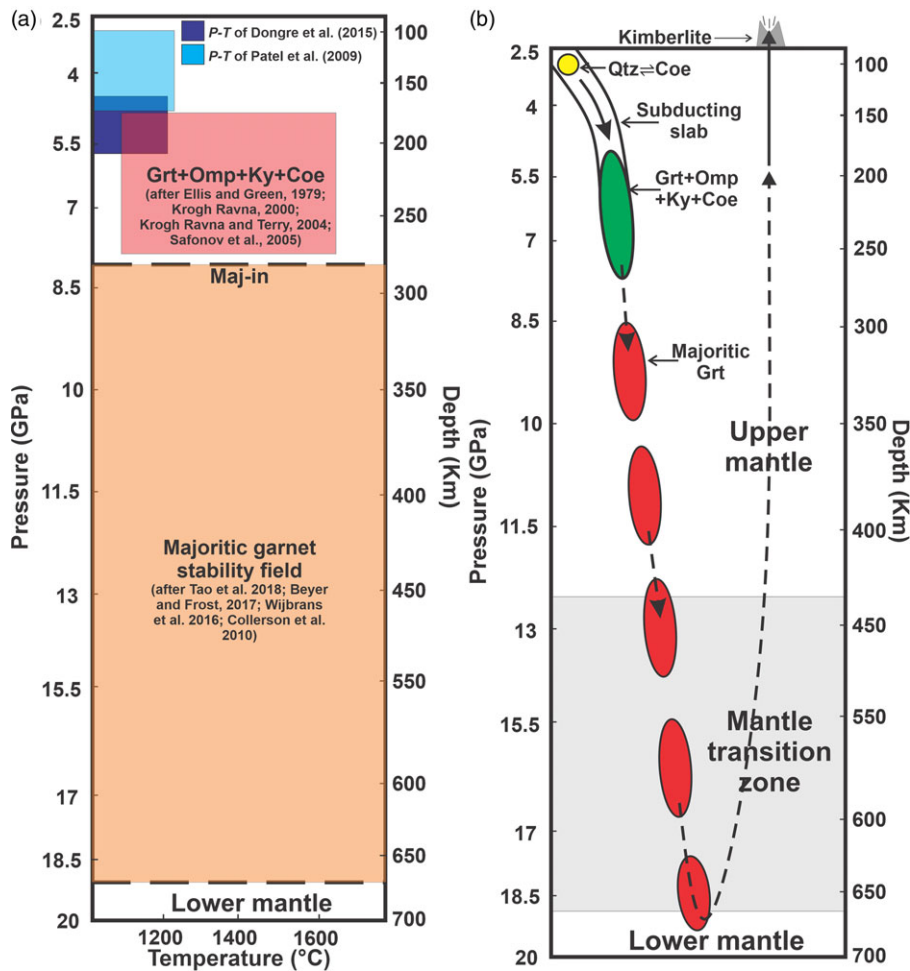


**Fig. 11.** (Colour online) (a) A pressure–temperature–depth diagram showing the evolution of the subducting crust up to the mantle transition zone. Previous *P–T* estimation from the eclogite xenoliths of pipe KL-2 is also shown for a comparative understanding. (b) A simplistic diagram showing formation of coesite, K-omphacite and majoritic garnet with increasing depth due to subduction, and a probable transportation path of majoritic garnet from the base of the mantle transition zone (shaded in grey) to the crust through kimberlite eruption.

#### 5.d. Origin and evolution of the Kalyandurg eclogite

The geothermobarometric estimations obtained from the coarse-grained garnet and omphacite pair, which are in textural equilibrium with kyanite and coesite, revealed that the eclogite formed at ~5–8 GPa pressure. Thus, the depth of subducted crustal material is estimated as ~175–280 km. Subsequently, owing to the continued subduction or sinking of the subducted crust after slab break-off, deeper than 280 km, the omphacite and coarse-grained garnet dissociated to form Na–Ca-rich majoritic garnet along the rim of the omphacite and coarse-grained garnet due to increasing pressure. The geobarometric estimations obtained from the majoritic garnet revealed the formation pressure to be 8–19 GPa, which translates to the depth range of ~280–660 km. Thus, combining the textural observations with geobarometric estimations, it is inferred that the eclogite, once formed owing to ultra-deep subduction between 175 and 280 km, travelled through the mantle transition zone up to ~660 km, which is manifested by the formation of majoritic garnet from the omphacite and coarse-grained garnet. Hence, this kimberlite-borne eclogite xenolith from the Kalyandurg cluster provides a unique opportunity to investigate the evolution of a subducted crust up to the mantle transition zone.

The studied sample preserves a plethora of UHP minerals that individually bear records of different equilibration depths. For example, quartz to coesite transformation occurred at >100 km (Fig. 11b), whereas the characteristic eclogitic assemblage (garnet–omphacite–kyanite–rutile) formed between 175 and 280 km

(Fig. 11b). Continuous increment of pressure after ~280 km, transformed the omphacite and coarse-grained garnet into majoritic garnet up to ~660 km (Fig. 11b). Subsequently, after reaching a depth of 660 km up to the mantle transition zone, the eclogite xenolith was brought back to the surface by a kimberlite eruption during Mesoproterozoic time (~1.1 Ga; Chalapathi Rao *et al.* 2013) (Fig. 11b). The ascent of eclogite xenoliths from such a great depth to the surface led Paton *et al.* (2007) to suggest that the kimberlite magma of the Kalyandurg cluster originated from the mantle transition zone. However, as the eclogitic lithologies are ductile at sublithospheric (convecting mantle) depths, it is difficult to expect such material to undergo fracturing and entrainment in the kimberlitic melt (see Tappe *et al.* 2020). It is speculated that the eclogite from the mantle transition zone was carried up rapidly to an intermediate depth (~200–300 km) by pre-Mesoproterozoic (>1.1 Ga) mantle plume activity that generated widespread mafic dykes in the Dharwar Craton (Samal *et al.* 2019). Such a rapid ascent of the mantle plume could possibly prevent the partial melting vis-à-vis melt loss from the eclogite, which in turn, helped to preserve the coesite, K-omphacite and majoritic garnet in the sample. Consequently, the kimberlite magma that originated from such a depth range (~200–300 km) carried the eclogite as a xenolith (Fig. 11b). The exact process(es) involved during the ascent of eclogite xenoliths from the mantle transition zone to the base of the lithosphere–asthenosphere boundary is difficult to establish and is beyond the scope of this work. Nevertheless, irrespective of the process(es) involved, it is certain that the kimberlite-borne

eclogite xenolith evolved near the mantle transition zone as a consequence of pre-Mesoproterozoic ultra-deep subduction before its entrainment in the ~1.1 Ga old Kalyandurg kimberlite.

**Acknowledgements.** NVCR thanks DST-SERB, New Delhi for a research project (IR/S4/ESF-18/2011 dated 12.11.2013). NVCR and RP are grateful to BHU for awarding an IoE incentive and Seed grant. AC thanks BHU for a Malaviya Post-Doctoral Fellowship (IoE/MPDF/2020-21/15). Analytical help by Prof. Satyeh Saha (Department of Chemistry, BHU) and Dr Koushik Sen (WIHG, Dehradun) is thoroughly acknowledged. Efficient editorial handling by Dr Tim Johnson and critical comments by the reviewer Dr Renée Tamblyn are much appreciated. A previous version of the manuscript was greatly benefited by the comments of Drs Sonja Aulbach, Katie Smart and an anonymous reviewer.

## References

- Akaogi M and Akimoto S** (1977) Pyroxene-garnet solid-solution equilibria in the systems  $Mg_4Si_4O_{12}$ - $Mg_3Al_2Si_3O_{12}$  and  $Fe_4Si_4O_{12}$ - $Fe_3Al_2Si_3O_{12}$  at high pressures and temperatures. *Physics of the Earth and Planetary Interiors* **15**, 90–106.
- Alifirova TA, Pokhilenko LN and Korsakov AV** (2015) Apatite,  $SiO_2$ , rutile and orthopyroxene precipitates in minerals of eclogite xenoliths from Yakutian kimberlites, Russia. *Lithos* **226**, 31–49.
- Angel RJ, Gasparik T, Ross NL, Finger LW, Prewitt CT and Hazen RM** (1988) A silica-rich sodium pyroxene phase with six-coordinated silicon. *Nature* **335**, 156–8.
- Aulbach S and Arndt NT** (2019) Eclogites as palaeodynamic archives: evidence for warm (not hot) and depleted (but heterogeneous) Archaean ambient mantle. *Earth and Planetary Science Letters* **505**, 162–72.
- Aulbach S and Jacob DE** (2016) Major- and trace-elements in cratonic mantle eclogites and pyroxenites reveal heterogeneous sources and metamorphic processing of low-pressure protoliths. *Lithos* **262**, 586–605.
- Babu EVSSK, Griffin WL, Panda S, O'Reilly SY and Bhaskar Rao YJ** (2008) Eclogite xenoliths from the kimberlites of the Eastern Dharwar craton, South India: material representing ancient crust of the Western Dharwar craton? *International Kimberlite Conference Extended Abstracts* **9**. doi: [10.29173/ikc3405](https://doi.org/10.29173/ikc3405).
- Beyer C and Frost DJ** (2017) The depth of sub-lithospheric diamond formation and the redistribution of carbon in the deep mantle. *Earth and Planetary Science Letters* **461**, 30–9.
- Beyer C, Frost DJ and Miyajima N** (2015) Experimental calibration of a garnet-clinopyroxene geobarometer for mantle eclogites. *Contributions to Mineralogy and Petrology* **169**, 18. doi: [10.1007/s00410-015-1113-z](https://doi.org/10.1007/s00410-015-1113-z).
- Bindi L, Safonov OG, Yapaskurt VO, Perchuk LL and Menchetti S** (2003) Ultrapotassic clinopyroxene from the Kumdy-Kol microdiamond mine, Kokchetav Complex, Kazakhstan: occurrence, composition and crystal-chemical characterization. *American Mineralogist* **88**, 464–8.
- Chadwick B, Vasudev VN and Hegde GV** (2000) The Dharwar craton, southern India, interpreted as the result of Late Archaean oblique convergence. *Precambrian Research* **99**, 91–111.
- Chalapathi Rao NV, Creaser RA, Lehmann B and Panwar BK** (2013) Re–Os isotopic study of Indian kimberlites and lamproites: implications for mantle source regions and cratonic evolution. *Chemical Geology* **353**, 36–47.
- Chalapathi Rao NV, Dongre A, Wu F-Y and Lehmann B** (2016) A Late Cretaceous (ca. 90 Ma) kimberlite event in southern India: implication for sub-continental lithospheric mantle evolution and diamond exploration. *Gondwana Research* **35**, 378–89.
- Collerson KD, Williams Q, Kamber BS, Omori S, Arai H and Ohtani E** (2010) Majoritic garnet: a new approach to pressure estimation of shock events in meteorites and the encapsulation of sub-lithospheric inclusions in diamond. *Geochimica et Cosmochimica Acta* **74**, 5939–57.
- Day HW and Mulcahy SR** (2007) Excess silica in omphacite and the formation of free silica in eclogite. *Journal of Metamorphic Geology* **25**, 37–50.
- Dongre A, Jacob DE and Stern RA** (2015) Subduction-related origin of eclogite xenoliths from the Wajrakarur kimberlite field, Eastern Dharwar craton, Southern India: constraints from petrology and geochemistry. *Geochimica et Cosmochimica Acta* **166**, 165–88.
- Dongre A, Lavhale P and Li Q-L** (2021) Perovskite U–Pb age and petrogenesis of the P-12 kimberlite from the Eastern Dharwar craton, southern India: implications for a possible linkage to the 1110 Ma large igneous province. *Journal of Asian Earth Sciences* **213**, 104750. doi: [10.1016/j.jseas.2021.104750](https://doi.org/10.1016/j.jseas.2021.104750).
- Doukhan N, Sautter V and Doukhan JC** (1994) Ultradeep, ultramafic mantle xenoliths: transmission electron microscopy preliminary results. *Physics of the Earth and Planetary Interiors* **82**, 195–207.
- Ellis DJ and Green DH** (1979) An experimental study of the effect of Ca upon garnet-clinopyroxene Fe–Mg exchange equilibria. *Contributions to Mineralogy and Petrology* **71**, 13–22.
- Friend CRL and Nutman AP** (1991) SHRIMP U–Pb geochronology of the Closepet Granite and Peninsular Gneiss, Karnataka, South India. *Journal of the Geological Society of India* **8**, 357–68.
- Ghosh S, Tiwari K, Miyahara M, Rohrbach A, Vollmer C, Stagno V, Ohtani E and Ray D** (2021) Natural Fe-bearing aluminous bridgmanite in the Katol L6 chondrite. *Proceedings of the National Academy of Sciences* **118**, e2108736118. doi: [10.1073/pnas.2108736118](https://doi.org/10.1073/pnas.2108736118).
- Gillet P, Sautter V, Harris J, Reynard B, Harte B and Kunz M** (2002) Raman spectroscopic study of garnet inclusions in diamonds from the mantle transition zone. *American Mineralogist* **87**, 312–17.
- Gonzalez JP, Baldwin SL, Thomas JB, Nachlas WO and Fitzgerald PG** (2020) Evidence for ultrahigh-pressure metamorphism discovered in the Appalachian orogen. *Geology* **48**, 947–51.
- Gupta S, Rai SS, Prakasam KS, Srinagesh D, Bansal BK, Chadha RK, Priestley K and Gaur VK** (2003) The nature of the crust in southern India: implications for Precambrian crustal evolution. *Geophysical Research Letters* **30**. 1419. doi: [10.1029/2002GL016770](https://doi.org/10.1029/2002GL016770).
- Haggerty SE and Birkett T** (2004) Geological setting and chemistry of kimberlite clan rocks in the Dharwar Craton, India. *Lithos* **76**, 535–49.
- Haggerty SE and Sautter V** (1990) Ultradeep (greater than 300 kilometres), ultramafic upper mantle xenoliths. *Science* **248**, 993–6.
- Harlow GE** (1997) K in clinopyroxene at high pressure and temperature: an experimental study. *American Mineralogist* **82**, 259–69.
- Harlow GE and Veblen DR** (1991) Potassium in clinopyroxene inclusions from diamonds. *Science* **251**, 652–5.
- Hatch DM and Ghose S** (1989) Symmetry analysis of the phase transition and twinning in  $MgSiO_3$  garnet: implications to mantle mineralogy. *American Mineralogist* **74**, 1221–24.
- Hills DV and Haggerty SE** (1989) Petrochemistry of eclogites from the Koidu Kimberlite Complex, Sierra Leone. *Contributions to Mineralogy and Petrology* **103**, 397–422. doi: [10.1007/BF01041749](https://doi.org/10.1007/BF01041749).
- Hirose K, Fei Y, Ma Y and Mao HK** (1999) The fate of subducted basaltic crust in the Earth's lower mantle. *Nature* **397**, 53–6.
- Hofmeister AM, Giesting PA, Wopenka B, Gwanmesia GD and Jolliff BL** (2004) Vibrational spectroscopy of pyrope-majorite garnets: structural implications. *American Mineralogist* **89**, 132–46.
- Irifune T** (1987) An experimental investigation of the pyroxene-garnet transformation in a pyrolite composition and its bearing on the constitution of the mantle. *Physics of the Earth and Planetary Interiors* **45**, 324–36.
- Jacob D** (2004) Nature and origin of eclogite xenoliths from kimberlites. *Lithos* **77**, 295–316.
- Jacob DE, Schmickler B and Schulze DJ** (2003) Trace element geochemistry of coesite-bearing eclogites from the Roberts Victor kimberlite, Kaapvaal craton. *Lithos* **71**, 337–51.
- Jaques AL, O'Neill HStC, Smith CB, Moon J and Chappell BW** (1990) Diamondiferous peridotite xenoliths from the Argyle (AK1) lamproite pipe, Western Australia. *Contributions to Mineralogy and Petrology* **104**, 255–76.
- Jayananda M, Aadhiseshan KR, Kusiak MA, Wilde SA, Sekhama K-U, Guitreau M, Santosh M and Gireesh RV** (2020) Multi-stage crustal growth and Neorchaean geodynamics in the Eastern Dharwar Craton, southern India. *Gondwana Research* **78**, 228–60.
- Jayananda M, Santosh M and Aadhiseshan KR** (2018) Formation of Archaean (3600–2500 Ma) continental crust in the Dharwar Craton, southern India. *Earth-Science Reviews* **181**, 12–42.

- Kaminsky FV, Zakharchenko OD, Griffin WL, Channer DM and Khachatryan-Blinova GK (2000) Diamond from the Guaniamo area, Venezuela. *The Canadian Mineralogist* **38**, 1347–70.
- Karmalkar NR, Duraiswami RA, Chalapathi Rao NV and Paul DK (2009) Mantle-derived mafic-ultramafic xenoliths and the nature of Indian subcontinental lithosphere. *Journal of the Geological Society of India* **73**, 657–79.
- Katayama I, Parkinson CD, Okamoto K, Nakajima Y and Maruyama S (2000) Supersilicic clinopyroxene and silica exsolution in UHPM eclogite and pelitic gneiss from the Kokchetav massif, Kazakhstan. *American Mineralogist* **85**, 1368–74.
- Kavanagh JL and Sparks RSJ (2009) Temperature changes in ascending kimberlite magma. *Earth and Planetary Science Letters* **286**, 404–13.
- Kelley SP and Wartho J-A (2000) Rapid kimberlite ascent and the significance of Ar-Ar ages in xenolith phlogopites. *Science* **289**, 609–10.
- Krmíček L, Magna T, Pandey A, Chalapathi Rao NV and Kynický J (2022) Lithium isotopes in kimberlites, lamproites and lamprophyres as tracers of source components and processes related to supercontinent cycles. In *Lamprophyres, Lamproites and Related Rocks: Tracers to Supercontinent Cycles and Metallogenesis* (eds L Krmíček and NV Chalapathi Rao), pp. 209–36. Geological Society of London, Special Publication no. 513. doi: [10.1144/SP513-2021-60](https://doi.org/10.1144/SP513-2021-60).
- Krogh Ravna E (2000) The garnet–clinopyroxene Fe<sup>2+</sup>–Mg geothermometer: an updated calibration. *Journal of Metamorphic Geology* **18**, 211–19. doi: [10.1046/j.1525-1314.2000.00247.x](https://doi.org/10.1046/j.1525-1314.2000.00247.x).
- Krogh Ravna EJ and Paquin J (2003) Thermobarometric methodologies applicable to eclogites and garnet ultrabasites. *EMU Notes in Mineralogy* **5**, 229–59.
- Krogh Ravna EJ and Terry MP (2004) Geothermobarometry of UHP and HP eclogites and schists—an evaluation of equilibria among garnet–clinopyroxene–kyanite–phengite–coesite/quartz. *Journal of Metamorphic Geology* **22**, 579–92.
- Kumar A, Heaman LM and Manikyamba C (2007) Mesoproterozoic kimberlites in south India: a possible link to ~1.1 Ga global magmatism. *Precambrian Research* **154**, 192–204.
- Kunz M, Gillet P, Fiquet G, Sautter V, Graafsmas H, Conrad P and Harris J (2002) Combined in situ X-ray diffraction and Raman spectroscopy on majoritic garnet inclusions in diamonds. *Earth and Planetary Science Letters* **198**, 485–93.
- Mikhailenko D, Golovin A, Korsakov A, Aulbach S, Gerdes A and Ragozin A (2020) Metasomatic evolution of coesite-bearing diamondiferous eclogite from the Udachnaya kimberlite. *Minerals* **10**, 383. doi: [10.3390/min10040383](https://doi.org/10.3390/min10040383).
- Mikhailenko DS, Aulbach S, Korsakov AV, Golovin AV, Malygina EV, Gerdes A, Stepanov AS and Xu YG (2021) Origin of graphite–diamond-bearing eclogites from Udachnaya kimberlite pipe. *Journal of Petrology* **62**, egab033. doi: [10.1093/petrology/egab033](https://doi.org/10.1093/petrology/egab033).
- Moore RO and Gurney JJ (1985) Pyroxene solid solution in garnets included in diamond. *Nature* **318**, 553–5.
- Mosenfelder JL, Schertl H-P, Smyth JR and Liou JG (2005) Factors in the preservation of coesite: the importance of fluid infiltration. *American Mineralogist* **90**, 779–89.
- Navon O, Hutcheon ID, Rossman GR and Wasserburg GJ (1988) Mantle-derived fluids in diamond micro-inclusions. *Nature* **335**, 784–9.
- Nayak SS and Kudari SAD (1999) Discovery of diamond-bearing kimberlites in Kalyandurg area, Anantapur district, Andhra Pradesh. *Current Science* **76**, 1077–1079.
- Nehru CE and Reddy AK (1989) Ultramafic xenoliths from Wajrakarur kimberlites, India. *Geological Society of Australia Special Publication* **14**, 745–58.
- Okamoto K, Liou JG and Ogasawara Y (2000) Petrology of the diamond-grade eclogite in the Kokchetav Massif, northern Kazakhstan. *Island Arc* **9**, 379–99.
- Palin RM and Santosh M (2021) Plate tectonics: what, where, why, and when? *Gondwana Research* **100**, 3–24.
- Pandey A and Chalapathi Rao NV (2020) Supercontinent transition as a trigger for ~1.1 Gyr diamondiferous kimberlites and related magmatism in India. *Lithos* **370–371**, 105620. doi: [10.1016/j.lithos.2020.105620](https://doi.org/10.1016/j.lithos.2020.105620).
- Patel SC, Ravi S, Anil Kumar Y, Naik A, Thakur SS, Pati JK and Nayak SS (2009) Mafic xenoliths in Proterozoic kimberlites from Eastern Dharwar Craton, India: mineralogy and P–T regime. *Journal of Asian Earth Sciences* **34**, 336–46.
- Patel SC, Ravi S, Thakur SS, Rao TK and Subbarao KV (2006) Eclogite xenoliths from Wajrakarur kimberlites, southern India. *Mineralogy and Petrology* **88**, 363–80.
- Paton C, Hergt JM, Phillips D, Woodhead JD and Shee SR (2007) New insights into the genesis of Indian kimberlites from the Dharwar Craton via in situ Sr isotope analysis of groundmass perovskite. *Geology* **35**, 1011–14.
- Perrillat JP, Daniel I, Lardeaux JM and Cardon H (2003) Kinetics of the coesite–quartz transition: application to the exhumation of ultrahigh-pressure rocks. *Journal of Petrology* **44**, 773–88.
- Pokhilenko NP, Sobolev NV, Reutsky VN, Hall AE and Taylor LA (2004) Crystalline inclusions and C isotope ratios in diamonds from the Snap Lake/King Lake kimberlite dyke system: evidence of ultradeep and enriched lithospheric mantle. *Lithos* **77**, 57–67.
- Prinz M, Manson DV, Hlava PF and Keil K (1975) Inclusions in diamonds: garnet lherzolite and eclogite assemblages. *Physics and Chemistry of the Earth* **9**, 797–815.
- Ramakrishnan M and Vaidyanadhan R (2010) *Geology of India (Vol. 1 & 2)*. Bangalore: Geological Society of India.
- Roermund V and Drury MR (1998) Ultra-high pressure (P > 6 GPa) garnet peridotites in Western Norway: exhumation of mantle rocks from > 185 km depth. *Terra Nova* **10**, 295–301.
- Safonov OG, Bindi L and Vinograd VL (2011) Potassium-bearing clinopyroxene: a review of experimental, crystal chemistry and thermodynamic data with petrological applications. *Mineralogical Magazine* **75**, 2467–84.
- Safonov OG, Butvina V and Limanov E (2019) Phlogopite-forming reactions as indicators of metasomatism in the lithospheric mantle. *Minerals* **9**, 685. doi: [10.3390/min9110685](https://doi.org/10.3390/min9110685).
- Safonov OG, Perchuk LL and Litvin YA (2005) Equilibrium K-bearing clinopyroxene–melt as a model for barometry of mantle-derived mineral assemblages. *Russian Geology and Geophysics* **46**, 1318–34.
- Samal AK, Srivastava RK, Ernst RE and Söderlund U (2019) Neoproterozoic Mesoproterozoic mafic dyke swarms of the Indian shield mapped using Google Earth™ images and ArcGIS™, and links with large igneous provinces. In *Dyke Swarms of the World: A Modern Perspective*. (eds RK Srivastava, R Ernst and P Peng), pp. 335–90. Singapore: Springer. doi: [10.1007/978-981-13-1666-1\\_9](https://doi.org/10.1007/978-981-13-1666-1_9).
- Sautter V, Haggerty SE and Field S (1991) Ultradeep (>300 kilometres) ultramafic xenoliths: petrological evidence from the transition zone. *Science* **252**, 827–30.
- Schmickler B, Jacob DE and Foley SF (2004) Eclogite xenoliths from the Kuruman kimberlites, South Africa: geochemical fingerprinting of deep subduction and cumulate processes. *Lithos* **75**, 173–207.
- Schmidberger SS, Simonetti A, Heaman LM, Creaser RA and Whiteford S (2007) Lu–Hf, in-situ Sr and Pb isotope and trace element systematics for mantle eclogites from the Diavik diamond mine: evidence for Paleoproterozoic subduction beneath the Slave craton, Canada. *Earth and Planetary Science Letters* **254**, 55–68.
- Schulze DJ and Helmstaedt H (1988) Coesite–sanidine eclogites from kimberlite: products of mantle fractionation or subduction? *The Journal of Geology* **96**, 435–43.
- Schulze DJ, Valley JW and Spicuzza MJ (2000) Coesite eclogites from the Roberts Victor kimberlite, South Africa. *Lithos* **54**, 23–32.
- Shaikh AM, Patel SC, Ravi S, Behera D and Pruseth KL (2017) Mineralogy of the TK1 and TK4 ‘kimberlites’ in the Timmasamudram cluster, Wajrakarur Kimberlite Field, India: implications for lamproite magmatism in a field of kimberlites and ultramafic lamprophyres. *Chemical Geology* **455**, 208–30.
- Shirey SB and Richardson SH (2011) Start of the Wilson Cycle at 3 Ga shown by diamonds from subcontinental mantle. *Science* **333**, 434–6.
- Shu Q, Brey GP, Hofer HE, Zhao Z and Pearson DG (2016) Kyanite/corundum eclogites from the Kaapvaal Craton: subducted troctolites and layered

- gabbros from the Mid-to Early Archean. *Contributions to Mineralogy and Petrology* **171**, 11. doi: [10.1007/s00410-015-1225-5](https://doi.org/10.1007/s00410-015-1225-5).
- Smyth JR, Caporuscio FA and McCormick TC** (1989) Mantle eclogites: evidence of igneous fractionation in the mantle. *Earth and Planetary Science Letters* **93**, 133–41.
- Snyder GA, Taylor LA, Crozaz G, Halliday AN, Beard BL, Sobolev VN and Sobolev NV** (1997) The origins of Yakutian eclogite xenoliths. *Journal of Petrology* **38**, 85–113.
- Sobolev NV** (1977) *Deep-Seated Inclusions in Kimberlites and the Problem of the Composition of the Upper Mantle*. American Geophysical Union, Special Publication vol. 11. Washington DC, USA.
- Sobolev VN, McCammon CA, Taylor LA, Snyder GA and Sobolev NV** (1999) Precise Mössbauer milliprobe determination of ferric iron in rock-forming minerals and limitations of electron microprobe analysis. *American Mineralogist* **84**, 78–85.
- Stachel T, Brey GP and Harris JW** (2000) Kankan diamonds (Guinea) I: from the lithosphere down to the transition zone. *Contributions to Mineralogy and Petrology* **140**, 1–15.
- Stachel T and Harris JW** (2008) The origin of cratonic diamonds – constraints from mineral inclusions. *Ore Geology Reviews* **34**, 5–32.
- Stähle V, Altherr R, Nasdala L and Ludwig T** (2011) Ca-rich majorite derived from high-temperature melt and thermally stressed hornblende in shock veins of crustal rocks from the Ries impact crater (Germany). *Contributions to Mineralogy and Petrology* **161**, 275–91.
- Tao R, Fei Y, Bullock ES, Xu C and Zhang L** (2018) Experimental investigation on Fe<sup>3+</sup>-rich majoritic garnet and its effect on majorite geobarometer. *Geochimica et Cosmochimica Acta* **225**, 1–16.
- Tappe S, Budde G, Stracke A, Wilson A and Kleine T** (2020) The tungsten-182 record of kimberlites above the African superplume: exploring the links to the core-mantle boundary. *Earth and Planetary Science Letters* **547**, 116473. doi: [10.1016/j.epsl.2020.116473](https://doi.org/10.1016/j.epsl.2020.116473).
- Tappert R, Stachel T, Harris JW, Muehlenbachs K, Ludwig T and Brey GP** (2005) Subducting oceanic crust: the source of deep diamonds. *Geology* **33**, 565–8.
- Thompson AR, Kohn SC, Prabhu A and Walter MJ** (2021) Evaluating the formation pressure of diamond-hosted majoritic garnets: a machine learning majorite barometer. *Journal of Geophysical Research: Solid Earth* **126**, e2020JB020604. doi: [10.1029/2020JB020604](https://doi.org/10.1029/2020JB020604).
- Tomioka N, Fujino K, Ito E, Katsura T, Sharp T and Kato T** (2002) Microstructures and structural phase transition in (Mg, Fe) SiO<sub>3</sub> majorite. *European Journal of Mineralogy* **14**, 7–14.
- Tomioka N and Kimura M** (2003) The breakdown of diopside to Ca-rich majorite and glass in a shocked H chondrite. *Earth and Planetary Science Letters* **208**, 271–8.
- Usui T, Nakamura E, Kobayashi K, Maruyama S and Helmstaedt H** (2003) Fate of the subducted Farallon plate inferred from eclogite xenoliths in the Colorado Plateau. *Geology* **31**, 589–92.
- Van Roermund HLM, Drury MR, Barnhoorn A and De Ronde AA** (2000) Super-silicic garnet microstructures from an orogenic garnet peridotite, evidence for an ultra-deep (>6 GPa) origin. *Journal of Metamorphic Geology* **18**, 135–47.
- Viljoen KS** (1995) Graphite-and diamond-bearing eclogite xenoliths from the Bellsbank kimberlites, Northern Cape, South Africa. *Contributions to Mineralogy and Petrology* **121**, 414–23.
- Wijbrans CH, Rohrbach A and Klemme S** (2016) An experimental investigation of the stability of majoritic garnet in the Earth's mantle and an improved majorite geobarometer. *Contributions to Mineralogy and Petrology* **171**, 50. doi: [10.1007/s00410-016-1255-7](https://doi.org/10.1007/s00410-016-1255-7).
- Xie Z and Sharp TG** (2007) Host rock solid-state transformation in a shock-induced melt vein of Tenham L6 chondrite. *Earth and Planetary Science Letters* **254**, 433–45.
- Xu C, Kynicky J, Tao R, Liu X, Zhang L, Pohanka M, Song W and Fei Y** (2017) Recovery of an oxidized majorite inclusion from Earth's deep asthenosphere. *Science Advances* **3**. doi: [10.1126/sciadv.1601589](https://doi.org/10.1126/sciadv.1601589).
- Ye K, Liou JB, Cong B and Maruyama S** (2001) Overpressures induced by coesite-quartz transition in zircon. *American Mineralogist* **86**, 1151–5.
- Zhang L and Zhang G** (2021) Ultrahigh pressure metamorphism. *Encyclopedia of Geology* **2**, 553–60.
- Zhong X, Moulas E and Tajčmanová L** (2018) Tiny timekeepers witnessing high-rate exhumation process. *Scientific Reports* **8**, 2234. doi: [10.1038/s41598-018-20291-7](https://doi.org/10.1038/s41598-018-20291-7).